Research in Astronomy and Astrophysics, 24:095005 (10pp), 2024 September https://doi.org/10.1088/1674-4527/ad6db4

The Optical Variability Properties of TeV Blazars

Zi-An Su[1], Wen-Xin Yang[2,3,4], Xiang-Tao Zeng[2,3,4], Le-Jian Ou[2,3,4], Ze-Lin Li[5], Jiang-He Yang[6], and Jun-Hui Fan[2,3,4]
[1] Department of Physics, School of Physics and Electronics, Hunan Normal University, Changsha 410081, China
[2] Center for Astrophysics, Guangzhou University, Guangzhou 510006, China; fjh@gzhu.edu.cn
[3] Greater Bay Brand Center of the National Astronomical Data Center, Guangzhou 510006, China
[4] Astronomy Science and Technology Research Laboratory of Department of Education of Guangdong Province, Guangzhou 510006, China
[5] College of Microelectronics, Feicuihu Campus of Hefei University of Technology, Hefei 230601, China
[6] College of Mathematics and Physics Science, Hunan University of Arts and Science, Changde 415000, China
Received 2023 December 4; revised 2024 July 29; accepted 2024 August 6; published 2024 September 4

Abstract

Variability is one of the typical observational properties of blazars and the spectral changes are usually associated with variability, although this kind of association is unclear yet. In this work, we used data from the Steward Observatory blazar monitoring program to investigate the optical variability properties including the short-term timescale, the brightness-dependent spectral property, the correlation between the the brightness variation and the polarization, and then estimate the Doppler factors based on the obtained short timescale to study the polarization property for a sample of 20 TeV blazars. Our analyses arrive at the following results: (1) The largest variation amplitude in R-band, ΔR_M, covers a range from $\Delta R_M = 0.29$ mag (1ES 2344+514) to $\Delta R_M = 4.66$ mag (3C 279). (2) Intra-day variability was found from five sources with timescales from 0.14 day for S5 0716+714 to 0.98 day for PKS 2155–304. Sixteen sources show spectra that are bluer when they become brighter, suggesting a common bluer-when-brighter property. (3) The plot of the polarization versus estimated Doppler factor is consistent with the Doppler factor dependent formula of polarization. (4) The largest polarization is correlated with the largest optical variation, suggesting that the high polarization and high amplitude variation are both the indicator of beaming effect.

Key words: galaxies: active – galaxies: jets – radiation mechanisms: non-thermal

1. Introduction

Blazars are an extreme subclass of active galactic nuclei (AGNs) with many special observation properties, such as rapid and large amplitude variability, high and variable linear polarization, or strong γ-ray emissions and even TeV emissions and superluminal motions, etc. Those special observation properties are due to a beaming effect caused by the jet with a small viewing angle with respect to the line of observer's sight (Wills et al. 1992; Urry & Padovani 1995; Ghisellini et al. 2014; Acero et al. 2015; Zhang & Fan 2018; Xiao et al. 2019; Abdollahi et al. 2020; Ajello et al. 2020; Otero-Santos et al. 2020; Zhang et al. 2020; Zhou et al. 2021; Chen et al. 2022, 2023; Pei et al. 2022; Yang et al. 2022; Yang et al. 2022a, 2022b, 2023; Fan et al. 2023).

Blazars consist of two subclasses (BL Lac objects-BL Lacs and flat spectrum radio quasars-FSRQs) based on their emission line features. FSRQs have strong emission lines with equivalent width (EW) > 5 Å, while BL Lacs show no or only weak emission lines with EW < 5 Å. Ghisellini et al. (2012) proposed to use an accretion ratio, $\frac{L_{\rm BLR}}{L_{\rm Edd}} \sim 5 \times 10^{-4}$, to isolate BL Lacs from FSRQs. Recently, Zhang et al. (2022) adopted the Gaussian Mixture Modeling clustering method to calculate the ratio of $\log \frac{L_{\rm BLR}}{L_{\rm Edd}}$ for a sample of 449 Fermi blazars with available emissions lines and obtained that BL Lacs and FSRQs can be separated by $\log \frac{L_{\rm BLR}}{L_{\rm Edd}} = -3.15$. Pei et al. (2022) proposed that there is a changing look region called the "appareling zone" with $\log \frac{L_{\rm BLR}}{L_{\rm Edd}}$ being between -2.7 and -1.07, with those sources falling into the "appareling zone" are changing look blazars. However, it is also possible that the dividing line depends on the γ-ray luminosity (Xiao et al. 2022).

Padovani & Giommi (1995) proposed to use the peak frequency $\log \nu_{\rm p}$ of the spectral energy distribution (SED) to classify BL Lacs into high-frequency peaked BL Lacs (HBLs) and low-frequency peaked BL Lacs (LBLs), separated by $\log \nu_{\rm p}({\rm Hz}) = 15$. Ghisellini (1998) proposed that there is a subclass of BL Lacs with their synchrotron peak frequencies being higher than that of conventional HBLs, $\log \nu_{\rm p}({\rm Hz}) > 19$, which are called ultra-high-energy synchrotron peak BL Lacs (UHBLs; Costamante et al. 2001). By calculating the SEDs for a sample of 308 BL Lacs, Nieppola et al. (2006) classified BL Lac objects into LBLs, intermediate BL Lac objects (IBLs) and HBLs. Abdo et al. (2010) proposed that blazars can be classified as low synchrotron peak (LSP) source if $\log \nu_{\rm p}({\rm Hz}) \leqslant 14.0$, as an intermediate synchrotron peak (ISP) source if $14.0 < \log \nu_{\rm p}({\rm Hz}) \leqslant 15$, and as a high synchrotron peak (HSP) source if $\log \nu_{\rm p}({\rm Hz}) > 15$. Recently, Fan et al. (2016) calculated the SEDs for a sample of

1392 Fermi blazars and proposed that a source would be classified as an LSP source if $\log \nu_{\rm p}({\rm Hz}) \leqslant 14.0$, as an ISP source if $14.0 < \log \nu_{p}({\rm Hz}) \leqslant 15.3$, and as an HSP if $\log \nu_{p}({\rm Hz}) > 15.3$ (Fan et al. 2016). Later on, Yang et al. (2022) obtained $\log \nu_{\rm p}({\rm Hz}) \leqslant 13.7$ for LSPs, $13.7 < \log \nu_{p}({\rm Hz}) \leqslant 14.9$ for ISPs, and $\log \nu_{p}({\rm Hz}) > 14.9$ for HSPs.

Variability across the whole electromagnetic spectrum is a typical observation property of blazars (Fan et al. 2002, 2021; Gu et al. 2006; Yang et al. 2017; Xiang et al. 2018; Zhang et al. 2018, Zhang et al. 2023; Cai et al. 2022; Fang et al. 2022; Yuan et al. 2022; Lu et al. 2023; Otero-Santos et al. 2023). Fan et al. (2005) summarized the variability properties of blazars and pointed out that there are three types of variabilities based on the timescales: Short-term variability with timescale of minutes to days, which shed lights on the emission size and the black hole masses, the middle-term variability with timescales of weeks to months that may be caused by the spiral jet, and long-term variability with timescales of years, which may indicate the orbital period of a binary black hole system. The short-term variability timescale is also used to constrain the Doppler factor (Mattox et al. 1993; Cheng et al. 1999; Fan 2005; Fan et al. 2013; Pei et al. 2020). Observations show that it is common for the spectrum to change with the source brightness, generally BL Lacs indicate that the spectrum becomes bluer (harder) when the source becomes brighter (bluer when brighter, BWB), while FSRQs show that the spectrum becomes redder (softer) when the source becomes brighter (redder when brighter, RWB), and some sources show a complicated pattern (Gu et al. 2006; Zheng et al. 2008; Xiong et al. 2017; Gupta et al. 2018; Yuan et al. 2023). Variation is also observed in the polarization of blazars (Feigelson et al. 1986; Mead et al. 1990) and the polarization is found to be correlated with the core-dominance parameter (Wills et al. 1992; Fan et al. 2006), variation (Fan & Lin 2000), spectral index (Fan et al. 2008), and brightness (Mead et al. 1990).

As the generation that followed Energetic Gamma Ray Experiment Telescope (EGRET, Hartman et al. 1999), Fermi/Large Area Telescope (LAT) detected 3743 blazars and blazar candidates of uncertain type (BCUs) (Abdollahi et al. 2020; Ajello et al. 2020; Ballet et al. 2020). The γ-ray emission was also proposed to be one of the observational properties in blazars (Fan et al. 2013).

Emissions were also detected in TeV band for blazars. From TeVCat[7] (Wakely & Horan 2008), we can see that 81 blazars have TeV emissions, most of which are BL Lacs, particularly HSP BL Lacs. Compared to GeV blazars, the number of TeV blazars is only 3% that of GeV blazars. There are many works on the TeV candidate searches. Costamante & Ghisellini (2002) found that TeV BL Lacs occupy the region of both high radio and high X-ray fluxes and proposed that BL Lacs with strong radio and X-ray emissions are TeV candidates, and obtained 33 TeV BL Lac candidates. Massaro et al. (2013) found the TeV BL Lacs candidates have similar infrared (IR) color index range ($0.22\,{\rm mag} < [3.4\,\mu{\rm m}] - [4.6\,\mu{\rm m}] < 0.86\,{\rm mag}$ and $1.60\,{\rm mag} < [4.6\,\mu{\rm m}] - [12\,\mu{\rm m}] < 2.32\,{\rm mag}$) and $F_{\rm X} > 2.45 \times 10^{-12}\,{\rm erg\,cm^{-2}\,s^{-1}}$ as TeV BL Lacs. Massaro et al. (2013) predicted 95 TeV BL Lac candidates. Chang et al. (2017) proposed 1691 HSPs as TeV candidates. Very recently, Zhu et al. (2023) used machine learning methods and identified 40 high-confidence TeV candidates from 1459 blazars in 4FGL-DR2/4LAC-DR2. They calculated the SEDs for the 40 candidates and predicted one source (4FGL J1058.6+5627) can be detected by the Large High Altitude Air Shower Observatory ((LHAASO) in Zhu et al. 2023). More TeV BL Lac objects will provide us with opportunities to search for the TeV emission mechanisms in BL Lacs and study the nature of TeV BL Lacs.

Lin & Fan (2016) made comparisons in observational properties between TeV BL Lacs and non-TeV BL Lacs. They found that (1) TeV BL Lacs are different from LSP and ISP BL Lacs but show similar properties to HSP BLs. (2) TeV HSP BL Lacs and non-TeV HSP BL Lacs exhibit differences in their $\alpha_{\rm RO}$ and α_{γ} but basically share other properties. Recently, Liang et al. (2023) investigated the mid-infrared (mid-IR) properties of TeV blazars and non-TeV blazars and found that the TeV BL Lac objects have stronger mid-IR emissions than GeV blazars and the TeV emissions are correlated with the mid-IR emissions. A statistical investigation of TeV BL Lacs at the optical band may be also interesting for the TeV BL Lacs. However, most of the optical property studies are mainly for individual TeV sources: 2344+514 (Cai et al. 2022), BL Lacertae (Gaur et al. 2019; Jorstad et al. 2022; Kalita et al. 2023; Raiteri et al. 2023; Yuan et al. 2023), OJ 287 (Gupta et al. 2019), 3C 66A, S4 0954+658 (Gaur et al. 2019), etc. There are no statistical analyses for a sample of TeV BL Lacs. Thanks to the Steward Observatory (SO) spectropolarimetric monitoring project (SPOL), we can analyze optical photometric and polarimetric data in both V and R bands for blazars. This motivated us to do a statistical analysis of the optical properties for a sample of TeV BL Lacs.

In this work, we will investigate their optical variability properties based on the data of Smith et al. (2009). The work is arranged as follows. In Section 2, we describe the sample in this work. The analysis results are presented in Section 3 with discussion, and our conclusions are provided in the Section 4.

2. Sample and Results

In this work, we collected the optical V and R band photometric observations and polarization for a sample of 20 TeV blazars from the SO SPOL, which uses the 2.3 m Bok Telescope located on Kitt Peak and the 1.54 m Kuiper Telescope in Arizona (Smith et al. 2009) to monitor a sample of blazars, and listed them in Table 1.

[7] http://tevcat.uchicago.edu/

Fan & Lin (2000) obtained the de-reddened magnitude as follows. First, the Galactic latitude and longitude of each source were calculated; second, the location of each source on the Burstein & Heiles H I maps (Burstein & Heiles 1982) is used to determine the proper reddening $E(B-V)$; third, the extinction A_λ is determined from the relation $X(\eta)=A_\lambda/E(B-V)$, where $\eta=1/\lambda$ (see Seaton 1979) was used to correct the observation magnitude. Now, we can get the de-reddened V and R magnitudes from the website.[8] The corresponding values are listed in Column (3) and Column (4) for V and R bands in Table 1. The example light curves for four sources (3C 66A, 1ES 1959+650, BL Lac and ES 2344+514) are displayed in the left panels in Figure 1. Fifteen sources have V and R photometric magnitudes and five sources (TXS 0506+056, VER J0521+211, S4 0954+658, S3 1227+25, PG 1554+113) have only differential photometric data between the source (V_S, R_S) and the comparison stars (V_C, R_C), namely V_S-V_C and R_S-R_C.

From our collection, we found that the greatest V variation amplitude is in a range from $\Delta V=0.32$ mag in Mkn 501 to $\Delta V=4.71$ mag in 3C 279, and the greatest R variation magnitude is in a range from $\Delta R=0.29$ in Mkn 501 to $\Delta R=4.66$ in 3C 279. The greatest variation amplitude in V band tends to be larger than that in R band, suggesting greater variability in shorter wavelengths than in longer ones. For the color index, the maximum color-index $(V-R)_{\rm Max}$ is in a range from $(V-R)_{\rm Max}=0.09$ in TXS 0506+056 to $(V-R)_{\rm Max}=1.00$ in BL Lac, while the minimum color-index $(V-R)_{\rm min}$ is in a range from $(V-R)_{\rm min}=0.05$ in TXS 0506+056 to $(V-R)_{\rm min}=0.62$ in BL Lac.

In addition, it is also found that the color index is positively correlated with the greatest variation amplitude, $\Delta(V-R)=(0.01\pm0.07)\Delta R+(0.22\pm0.16)$ with a correlation coefficient of $r=0.05$ and a chance probability of $p=8.3\%$, as shown in Figure 2.

2.1. Spectrum and Brightness Correlation

Based on the corrected magnitudes and the corresponding color indexes, we can investigate the relationship between the magnitude and color index. One can see the light curve examples of four sources (3C 66A, 1959+650, BL Lac, and 2344+514) from the left panels of Figure 1. Examples of the spectrum and the brightness correlations are displayed in the right panels of Figure 1. The results for the linear regression analysis for color index $V-R$ and R magnitude are listed in Table 2. We can see that the 16 sources show positive correlations between $V-R$ and R, or between $((V_S-V_C)-(R_S-R_C))$ and (R_S-R_C) for those sources with only differential magnitudes, which means a BWB phenomenon. For the remaining four sources (TXS 0506 +056, S4 0954+658, H1426+428, and PG 1553+113), more observations are needed for further investigation.

[8] https://irsa.ipac.caltech.edu/applications/DUST/

3. Discussions

Variability is a typical observation property of blazars, and is observed over the whole electromagnetic spectrum (Caproni & Abraham 2004; Aleksić et al. 2011; Foschini et al. 2011; Graham et al. 2015; Wang et al. 2017, 2022; Xiong et al. 2017; Gupta et al. 2018; Liodakis et al. 2018; Zhang et al. 2018; Zhang et al. 2018; Zhang et al. 2020, 2023; Wang & Shi 2020; Fan et al. 2021; Jorstad et al. 2022; Yang et al. 2022a; Bachev et al. 2023). The rapid large amplitude variability is explained as the relativistic beaming effect. In this sense, the observed timescale ($\Delta t_{\rm ob.}$) is shortened as $\Delta t_{\rm ob.}=\Delta t_{\rm in.}/\delta$ while the observed flux density ($f_{\rm ob.}$) is boosted as $f_{\rm ob.}=\delta^{\lambda+\alpha}f_{\rm in.}$, here δ is the Doppler factor (boosting factor), λ stands for the jet morphology ($\lambda=3$ for a moving sphere jet and $\lambda=2$ for a continuous jet, see Lind & Blandford 1985), α stands for the spectral index ($f_\nu\propto\nu^{-\alpha}$), $\Delta t_{\rm in.}$ is the intrinsic timescale, and $f_{\rm in.}$ is the intrinsic flux density.

In this work, we obtained the V and R photometric data from the SO SPOL (Smith et al. 2009) and analyzed their variabilities and timescales as described in detail in the following subsections.

3.1. Correlation between the Spectrum and Brightness

Different spectral behaviors have been found for different sources. Gu et al. (2006) analyzed the *BVRI* band data of eight sources and found a clear anti-correlation between the color index and R magnitude, which is known as the BWB phenomenon. Zheng et al. (2008) analyzed the long-term optical monitoring of OJ 287 and found the same behavior. Liao et al. (2014) analyzed the long-term multi-band SED of 0716+714 and found that the SED peak frequency moves toward shorter wavelengths when the source gets brighter. Many sources like 0716+714, OJ 287, 3C 66A, BL Lac, and PKS 0420-01 by Gu et al. (2006), 3C 345 by Wu et al. (2011) and Villata et al. (2006), and 3C 454.3 by Zhai et al. (2011) have been found to exhibit the same BWB phenomenon. On the other hand, the IR and optical spectra of some sources like Mkn 421 (Carnerero et al. 2017) and 0235+164 (Romero et al. 2000) remain unchanged when the sources get brighter.

For the color index $V-R$ and the R magnitude, we investigated their relationship and found strong correlations for 16 sources, suggesting a brightness-dependent spectral phenomenon as discussed in the literatures (Gu et al. 2006; Zheng et al. 2008; Gupta et al. 2018; Li et al. 2021).

For the 20 sources, four sources (TXS 0506+056, S4 0954 +658, H1426+428, and 1553+113) do not have enough data, so we consider the other 16 sources. Among them, 3C 66A, J0521+211, S5 0716+714, OJ 287, Mrk 421, S3 1227+25, 3C 279, Mrk 501, 1ES 1959+650, PKS 2155–304, BL Lac, and 1ES 2344+514 show clear correlations between the color index $(V-R)$ and the R magnitude, indicating BWB. Moreover, Ton 599, W Com, and PKS 1510–089 indicate that the

Table 1
Sample of 20 TeV Blazars

4FGL Name	Other Name	A_V	A_R	z	$\Delta V_{\rm M}$	$\Delta R_{\rm M}$	$(V-R)_{\rm M}$	$(V-R)_{\rm m}$	ΔR	ΔT	$P \pm \sigma P$	$\delta_{\rm SSC}$	$\delta_{\rm EC}$	$\delta_{\rm L18}$
(1)	(2)	(3)	(4)	(5)	(6)	(7)	(8)	(9)	(10)	(11)	(12)	(13)	(14)	(15)
J0222.6+4302	3C 66A	0.231	0.183	0.444	1.860	1.820	0.420	0.290	0.16	1.002	19.68 ± 0.03	23.35	17.95	3.40
J0509.4+0542	TXS 0506+056	0.297	0.235	0.689	0.552	0.537	0.093	0.049	0.175	1.000	16.45 ± 0.07	32.89	13.95	14.67
J0521+2113	J0521+211	1.872	1.481	0.108	1.431	1.400	0.179	0.095	0.25	1.047	13.89 ± 0.15	26.43	11.44	1.20
J0721.9+7120	S5 0716+714	0.085	0.067	0.3	2.920	2.870	0.460	0.340	0.13	0.140	27.96 ± 0.02	89.09	27.41	31.33
J0739.2+0137	PKS 0736+01	0.375	0.297	0.18941	2.780	2.760	0.730	0.510	0.47	0.780	27.43 ± 0.14	41.74	8.14	11.44
J0854.8+2006	OJ 287	0.077	0.061	0.3056	2.540	2.460	0.520	0.400	0.14	0.179	36.54 ± 0.06	493.78	31.93	29.77
J0958.7+6534	S4 0954+658	0.328	0.259	0.368	0.332	0.325	0.040	0.004	0.3	1.000	19.66 ± 0.10	40.55	11.19	6.62 (a)
J1104.4+3812	Mrk 421	0.042	0.033	0.031	1.900	1.810	0.420	0.140	0.14	0.930	12.39 ± 0.03	25.39	21.07	2.03
J1159.5+2914	Ton 599	0.054	0.043	0.725	3.820	3.820	0.460	0.350	0.69	0.897	33.16 ± 0.09	84.62	18.08	32.92
J1221.4+2814	W Com	0.064	0.051	0.103	1.990	1.950	0.510	0.360	0.29	1.000	26.69 ± 0.07	6.93	6.02	2.67
J1230.2+2517	S3 1227+25	0.053	0.042	0.135	1.936	1.875	0.132	0.054	0.16	0.800	26.75 ± 0.09	29.20	9.90	6.82
J1256.1-0547	3C 279	0.078	0.062	0.536	4.710	4.660	0.570	0.250	0.16	0.253	34.50 ± 0.06	224.79	25.98	11.64
J1428.5+4240	H1426+428	0.034	0.027	0.129	0.520	0.540	0.820	0.570	0.15	1.000	2.23 ± 0.03	3.51	12.51	3.76 (b)
J1512.8-0906	PKS 1510–08	0.275	0.217	0.36	2.770	2.780	0.520	0.260	0.44	1.030	25.82 ± 0.09	5.77	5.59	32.14
J1555+1111	PG 1553+113	0.142	0.113	0.36	0.677	0.684	0.031	0.001	0.202	4	13.73 ± 0.05	1.29	10.78	11.22
J1653.8+3945	Mrk 501	0.052	0.041	0.0337	0.320	0.290	0.590	0.460	0.09	1.007	5.93 ± 0.04	8.57	11.24	0.23
J2000.0+6508	1ES 1959+650	0.474	0.375	0.047	1.490	1.410	0.470	0.280	0.24	5.030	8.53 ± 0.05	1.29	5.33	1.60
J2158.8–3013	PKS 2155–304	0.060	0.047	0.116	2.210	2.180	0.400	0.330	0.1	0.980	19.06 ± 0.08	5.33	13.66	4.15 (b)
J2202.7+4216	BL Lac	0.901	0.713	0.0686	2.930	2.820	1.000	0.620	0.24	1.000	26.08 ± 0.06	114.08	11.46	12.17
J2347.0+5141	1ES 2344+514	0.580	0.458	0.044	0.350	0.290	0.630	0.520	0.13	1.020	5.63 ± 0.08	9.85	8.78	1.33

Note. Column (1), gives the source name in FGL; Column (2), the other name; Column (3), Galactic extinction in V band (A_V); Column (4), Galactic extinction in R band (A_R); Column (5), redshift, z; Column (6), maximum variation in V band ($\Delta V_{\rm M}$); Column (7), maximum variation in R band ($\Delta R_{\rm M}$); Column (8), maximum variation in color index, $(V-R)_{\rm Max}$; Column (9), minimum variation in color index, $(V-R)_{\rm min}$; Column (10), variation in R band ΔR; Column (11), timescale (ΔT) in units of days for ΔR in Column (10), Column (12), polarization and related uncertainty, Column (13), Doppler factor estimated for SSC process, $\delta_{\rm SSC}$, Column (14), Doppler factor estimated for EC process, $\delta_{\rm EC}$, and Column (15), Doppler factor by Liodakis et al. (2018), values labeled by (a) are from Lähteenmäki & Valtaoja (1999) and those labeled by (b) are from Fan et al. (2014).

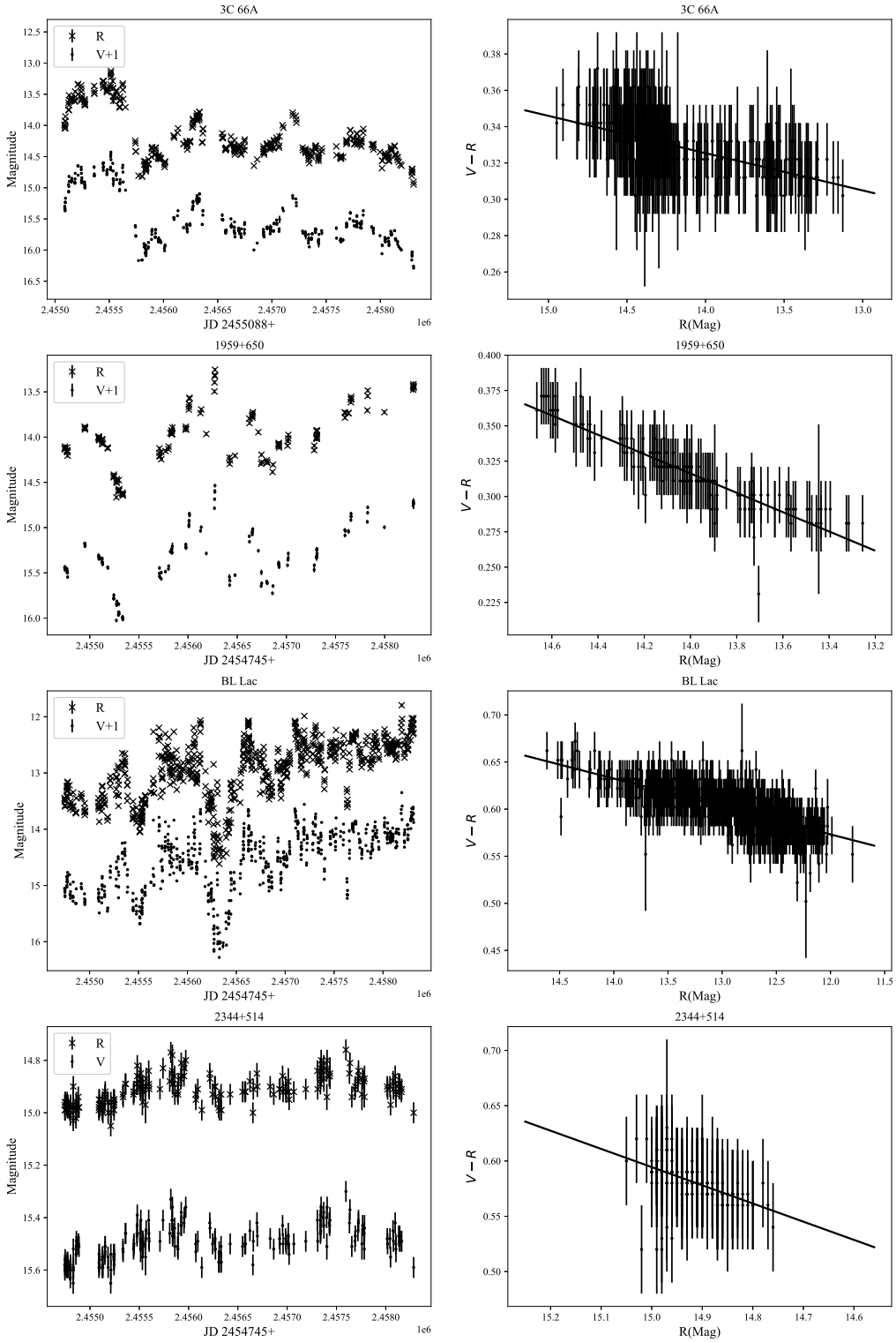

Figure 1. Light curves and the color index $V - R$ against R magnitude for four sources (from the top to the bottom are 3C 66A, 1ES 1959+650, BL Lac and 1ES 2344 +514, respectively).

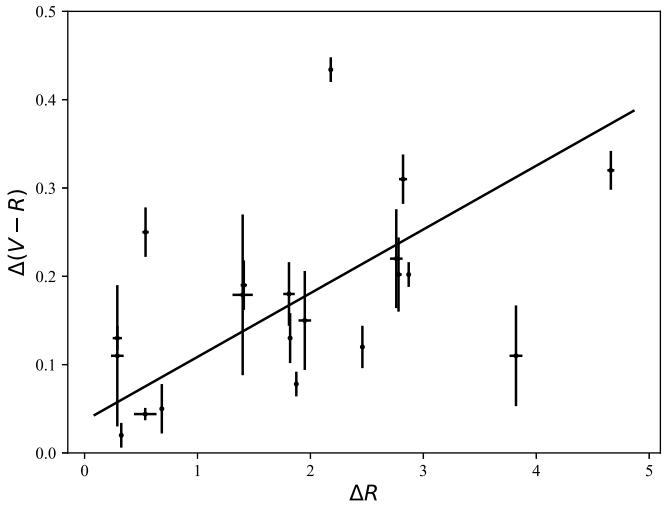

Figure 2. Plot of the color index $\Delta(V-R)$ against greatest R variability amplitude ΔR for our sample. The line stands for best fitting.

spectrum becomes redder when the brightness increases, suggesting a RWB phenomenon. For OJ 287, our BWB result is consistent with that by Gu et al. (2006) but different from that by Zheng et al. (2008). For 3C 66A, Mkn 421, and BL Lac, our BWB results are consistent with the results by Gu et al. (2006) and Meng et al. (2018). However, the spectrum did not change in Carnerero et al. (2017). For S5 0716+714, our BWB results are consistent with the results by Gu et al. (2006) and Poon et al. (2009). For 1ES 1959+650, our BWB result is consistent with the finding by Meng et al. (2018). For PKS 0736+01, it is found that there is no tendency for correlation between the color index $(V-R)$ and R magnitude, for which a chance probability of $p = 64\%$ was obtained. It is clear that the brightness-dependent phenomenon is complicated and worthy of further study using a larger sample. Fortunately, the Chinese Space Station Telescope (CSST) will provide us with a lot of simultaneous multiwavelength observations of AGNs, which will help astronomers to study and understand the nature of the brightness-dependent phenomenon.

In addition, we also found that the color index variability $\Delta(V-R)$ and the variability amplitude ΔR are closely correlated, as depicted in Figure 2. It is understandable if the spectrum changes with the brightness, so that the more violently a source varies, the larger the color index change. A similar phenomenon in the γ-ray band is discussed by Yang et al. (2022b), Yu et al. (2024).

3.2. Doppler Factor

Observations indicate a double bump structure for the SED for blazars (Urry & Padovani 1995; Abdo et al. 2010), the first bump is from the radio to X-ray band with the peak being at the IR to X-ray band, which is from the synchrotron emission of the relativistic electrons in the jet, while the second bump is from the X-ray band to the γ-ray band and the peak is at the X-ray to GeV γ-ray band; it is proposed to be from the inverse Compton (IC) emissions. Shaw et al. (2012) and Paliya et al. (2021) show that FSRQs have richer seed photons from the external field than BL Lacs through the emission line observations. The γ-ray emissions may be the combined result of the synchrotron self-Compton (SSC) and the external Compton (EC) process for FSRQs, while the SSC is the main mechanism for the γ-ray emissions in BL Lacs (Ghisellini et al. 1998).

The variability and the corresponding timescale are used to estimate the Doppler factor. Radio observations show that it is reasonable to define the equipartition brightness temperature (intrinsic brightness temperature) of blazars (Lähteenmäki & Valtaoja 1999; Hovatta et al. 2009); Savolainen et al. (2010) and Liodakis et al. (2018) estimated the variability Doppler factor for 1029 blazars based on long-term monitoring in radio band and intrinsic temperature. Xie et al. (1989, 1992) estimated the optical Doppler factor based on the idea that the difference between the observed mass energy conversion rate (η^{ob}) and the intrinsic rate (η^{in}) is from the boosting effect. The Doppler factor in the γ-ray band can be constrained by the geometry of the radiation zone (Mattox et al. 1993; von Montigny et al. 1995; Cheng et al. 1999; Fan 2005; Fan et al. 2013, 2014; Pei et al. 2020; Zhang et al. 2020; Wang et al. 2022; Yang et al. 2022a).

Table 2
Correlation Analysis Results

Source Name (1)	$a \pm \Delta a$ (2)	$b \pm \Delta b$ (3)	r (4)	p (5)
3C 66A	0.02 ± 0.002	0.06 ± 0.03	0.48	0
TXS 0506+056	-0.002 ± 0.02	0.01 ± 0.002	0.02	90%
VER J0521+211	0.02 ± 0.01	-0.25 ± 0.004	0.34	5.10×10^{-5}
S5 0716+714	0.01 ± 0.002	0.24 ± 0.03	0.40	6.64×10^{-10}
PKS 0736+01	-0.003 ± 0.006	0.55 ± 0.09	0.04	64%
OJ 287	0.02 ± 0.002	0.21 ± 0.03	0.40	0
Mrk 421	0.04 ± 0.001	-0.20 ± 0.02	0.80	0
Ton 599	-0.005 ± 0.002	0.49 ± 0.03	0.21	2.0×10^{-3}
W Com	-0.05 ± 0.007	1.09 ± 0.11	0.33	1.75×10^{-10}
S3 1227+25	0.03 ± 0.003	-0.14 ± 0.004	0.69	0
3C 279	0.02 ± 0.002	0.10 ± 0.02	0.53	0
H1426+428	0.05 ± 0.08	-0.16 ± 1.25	0.11	52%
PKS 1510-089	-0.02 ± 0.003	0.67 ± 0.05	0.34	1.52×10^{-11}
PG 1553+113	0.008 ± 0.01	-0.41 ± 0.002	0.10	42%
Mrk 501	0.11 ± 0.007	-0.98 ± 0.10	0.57	0
1ES1959+650	0.07 ± 0.01	-0.59 ± 0.07	0.76	0
PKS 2155-304	0.01 ± 0.001	0.22 ± 0.02	0.37	5.03×10^{-12}
BL Lac	0.03 ± 0.002	0.26 ± 0.02	0.47	0
1ES 2344+514	0.17 ± 0.02	-1.92 ± 0.30	0.50	1.6×10^{-13}
S4 0954+658	-0.01 ± 0.02	-0.01 ± 0.04	0.22	66%

Note. Column (1) Source name; Column (2) slope and related uncertainty; Column (3) intercept and related uncertainty; Column (4) probability.

Combining the IC mechanism and the variability timescale, one can also constrain the Doppler factor (Chen 2018). The SED calculations for the synchrotron component were carried out for the released catalogs by Fan et al. (2016) for a sample of 1392 Fermi blazars and by Yang et al. (2022) for a sample of 2709 Fermi blazars. For the high energy region, the SED calculations were performed by Yang et al. (2023) for 3743 Fermi blazars. Those calculations are useful for the emission mechanism investigation and the physics parameter constraints (Chen 2018; Fan et al. 2023).

According to properties of a soft photon, the Doppler factor in the Thomson regime can be estimated through SED parameters obtained by fitting a logarithmic parabola (Chen 2018)

$$\delta = 9.0365\left(\frac{\nu^p_{\rm sy}L(\nu^p_{\rm sy})}{10^{45}\ {\rm erg\ s^{-1}}}\right)^{1/4}\left(\frac{\nu^p_{\rm sy}}{10^{15}\ {\rm Hz}}\right)^{-1/2}\left(\frac{L_{\rm ssc}}{L_{\rm syn}}\right)^{-1/4} \times\left(\frac{\nu^p_{\rm ssc}}{10^{23}\ {\rm Hz}}\frac{10^{15}\ {\rm Hz}}{\nu^p_{\rm sy}}\right)^{1/2}\left(\frac{\Delta t(1+z)}{1\ {\rm day}}\right)^{-1/2}\left(\frac{b}{2}\right)^{-1/8}, \quad (1)$$

for the SSC process, or

$$\delta = 9.6321\left(\frac{\nu^p_{\rm ec}}{10^{22}\ {\rm Hz}}\frac{10^{14}\ {\rm Hz}}{\nu^p_{\rm sy}}\right)^{1/4}\left(\frac{\nu^p_{\rm sy}L(\nu^p_{\rm sy})}{10^{46}\ {\rm erg\ s^{-1}}}\right)^{1/8}\left(\frac{L_{\rm ssc}}{L_{\rm syn}}\right)^{-1/8} \times\left(\frac{\nu_{\rm ext}}{3\times10^{13}\ {\rm Hz}}\right)^{-1/4}\left(\frac{\Delta t(1+z)}{1\ {\rm day}}\right)^{-1/4}\left(\frac{b}{2}\right)^{-1/16}, \quad (2)$$

for the EC process.

In this sense, given the synchrotron peak frequency ($\nu^p_{\rm sy}$), synchrotron peak luminosity ($\nu^p_{\rm sy}L(\nu^p_{\rm sy})$) and the curvature for the synchrotron component (b), the peak frequency ($\nu^p_{\rm ssc}/\nu^p_{\rm ec}$) and the corresponding peak luminosity ($\nu^p_{\rm ssc}L(\nu^p_{\rm ssc})/\nu^p_{\rm ec}L(\nu^p_{\rm ec})$) for the Compton component can constrain the Doppler factor using the obtained timescale (Δt).

We obtained logarithmic parabola parameters for our sample from Yang et al. (2022), Yang et al. (2023). Using the timescale obtained in this work, we calculated the Doppler factors, $\delta_{\rm SSC}$ ($\delta_{\rm EC}$), for the SSC process (EC process) and listed them in Column (13) and Column (14) in Table 1 respectively.

For the SSC process, the Doppler factors cover from $\delta_{\rm SSC}=0.84$ (1ES 1959+650) to $\delta_{\rm SSC}=493.7$ (OJ 287), while those estimated from the EC process cover from $\delta_{\rm EC}=5.33$ (1ES 1959+650) to $\delta_{\rm EC}=31.93$ (OJ 287). Two other sources have Doppler factors greater than 100, which are 3C 279 ($\delta_{\rm SSC}=224.79$) and BL Lac $\delta_{\rm SSC}=114.08$.

The relationship between our Doppler factors and those from Liodakis et al. (2018) is investigated. We ascertained $\log\delta_{\rm SSC}=(0.64\pm0.29)\log\delta_{\rm L18}+(0.75\pm0.30)$ with $r=0.45$ and $p=4.5\%$, suggesting a weak positive correlation as visible in the upper panel of Figure 3, and $\log\delta_{\rm EC}=(0.14\pm0.09)\log\delta_{\rm L18}+(0.96\pm0.09)$ with $r=0.33$ and $p=15.3\%$, suggesting a positive correlation tendency as in the lower panel of Figure 3. It is clear that the sample is still too small, which results in a high chance probability. A larger sample will give a result with a higher confidence in the correlation analysis.

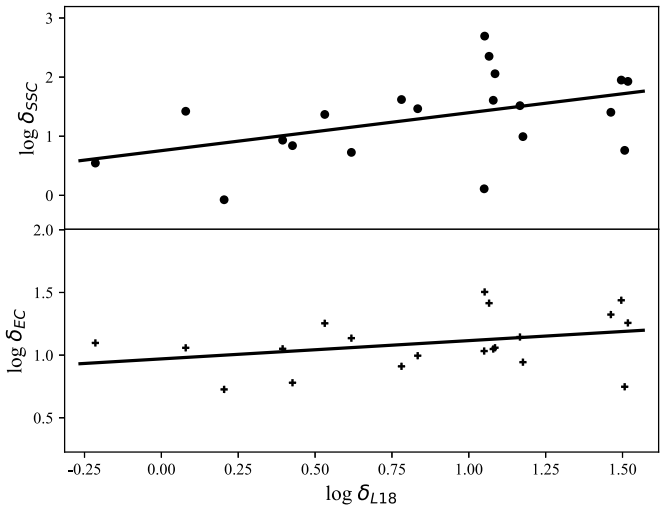

Figure 3. Correlations between our Doppler factors and the Doppler factors from the literature. The upper panel is for $\delta_{\rm SSC}$ versus δ in Liodakis et al. (2018), Fan et al. (2014), and the lower panel is for $\delta_{\rm EC}$ versus δ in Liodakis et al. (2018), Fan et al. (2014).

A large Doppler factor ($\delta>100$) also appeared in Chen (2018). The reason is perhaps from the fact that the physical parameters calculated for the two bumps are not very accurate. However, we can see the Doppler factors estimated from the EC process are not so large as those from the SSC process.

For the case of OJ 287, its $\delta_{\rm EC}=31.93$ is close to the value $\delta=29.77$ (Liodakis et al. 2018). For BL Lacertae, its $\delta_{\rm EC}=11.46$ is also close to the value $\delta=12.17$ (Liodakis et al. 2018). Does that mean the EC process is responsible for the γ-ray emissions or the EC process is the dominant mechanism for the γ-ray emissions? If this is the real case, then one can tell which mechanism is more important for the γ-ray emissions by comparing our Doppler factors with the Doppler factors in the literature.

Therefore, we will say that the EC process is the main process for the γ-ray emissions in TXS 0506+056, S5 0716 +714, OJ 287, Ton 599, 3C 279, 1553+113, and BL Lacertae, while the SSC process is the dominate process for the γ-ray emissions in PKS 0736+01, 1ES 1959+650, PKS 2155–304 and 1ES 2344+514. Both processes are responsible for the γ-ray emissions in 3C 66A, VER 0521+211, Mkn 421, Mkn 501, W Com, and 1510–089. We think that a larger sample with available variability timescale and the physical parameters from the SEDs will enable us to investigate the correlation between the estimated Doppler factors and the Doppler factors from the literature so that we can study the γ-ray emission mechanism.

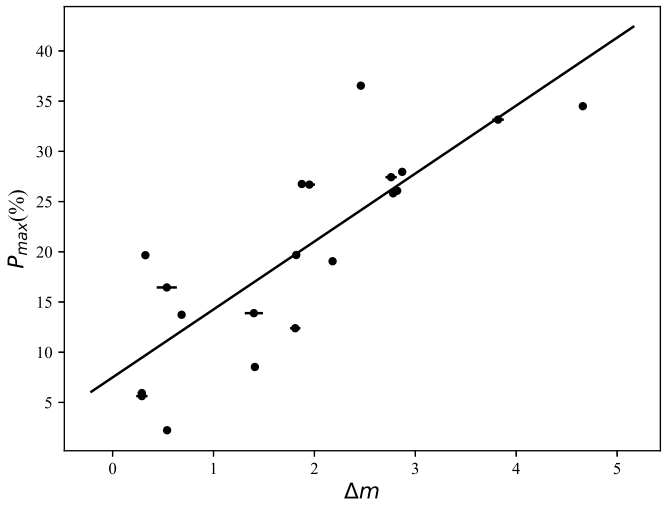

Figure 4. Plot of the largest optical polarization ($P_{\rm Max}(\%)$) versus the largest optical variation ($\Delta R_{\rm m}$).

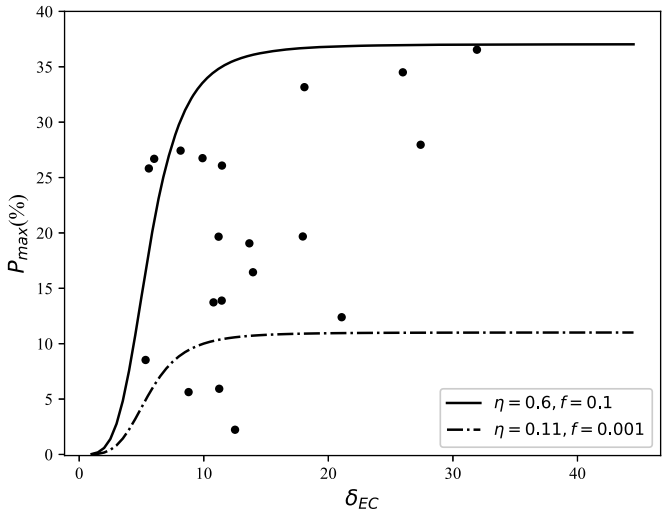

Figure 5. The largest optical polarization ($P_{\rm Max}(\%)$) versus the Doppler factor ($\delta_{\rm EC}$). The solid curve represents a theoretical result corresponding to $\eta = 0.6$ and $f = 0.1$, and the dash-dotted line is for a theoretical result for $\eta = 0.11$ and $f = 0.001$.

3.3. Polarization

In this work, the highest optical polarization is also collected from Smith et al. (2009) and listed in Column (12) in Table 1. When the linear regression analysis is performed for the polarization and the variation amplitude, a correlation is found, $P_{\rm Max}(\%) = (6.76 \pm 1.12)\Delta m + (7.49 \pm 2.47)$ with $r = 0.81$ and $p = 1.03 \times 10^{-5}$; the corresponding plot is shown in Figure 4. It suggests that higher polarization sources tend to have larger variation, as observed in Fan & Lin (2000).

Fan et al. (1997) derived a relation between the polarization ($P_{\rm ob}$) and the Doppler factor (δ)

$$P_{\rm ob} = \frac{f\delta^{\lambda}}{1 + f\delta^{\lambda}} P_{\rm in}, \tag{3}$$

where $P_{\rm in} = \frac{f}{1+f}\frac{\eta}{1+\eta}$ is the intrinsic polarization in the comoving frame, f is the ratio of the emission in the jet to the unbeamed emission in the comoving frame, and η is the ratio of the polarized emission to the unpolarized emission in the jet. Following Fan et al. (1997), we choose $\eta = 0.6, f = 0.1$ or $\eta = 0.11$, $f = 0.001$ and obtained the corresponding $P_{\rm in} = 0.1\%$ and 3.4%, then we could get the curves of P versus δ corresponding to $f = 0.001$ and $f = 0.1$ respectively. The two curves are displayed in Figure 5.

In the work, we used the collected maximum optical polarization listed in Column (12) in Table 1 and the estimated Doppler factor ($\delta_{\rm EC}$) to study the relation between them. The result is shown in Figure 5. The observation data follow the same tendency as the theoretical curves, suggesting that the polarization is an indication of the beaming effect or the high polarization is from the strong beaming effect in blazars. Most of the points are located in the region between the two curves, and the parameters for the two curves suggest the intrinsic polarizations for our sample are $P_{\rm in} = 0.1\%$ to 3.4%. In the discussion of the Doppler factor dependent polarization, it is hard to get the theoretical curve to fit the Doppler factor well since the parameter (f) differs from one source to another, showing a 5 dex difference for BL Lacs (Fan 2003). However, we suggest that the correlation can be tested using the simultaneous polarization and the corresponding Doppler factor for a selected source or a sample of similar type of sources. In this sense, the high observed polarization just suggests that the TeV blazars have strong beaming effect. For the 20 TeV blazars, 17 sources were given Doppler factor in the work by Liodakis et al. (2018), and nine sources have Doppler factors being greater than 10 as listed in Column (15) in Table 1.

4. Conclusion

In this work, we collected the optical V and R photometric observations and the optical polarizations for a sample of 20 TeV blazars, of which 15 sources have V and R magnitudes and the remaining five sources have only differential magnitudes between the sources and their comparison stars. Their optical variability timescales are investigated and used to estimate the Doppler factor. The Doppler factors are also compared with the known ones by Fan et al. (2014), Liodakis et al. (2018) and Lähteenmäki & Valtaoja (1999). Our conclusions are:

(1) The largest variation amplitude was obtained for all 20 TeV blazars with some having intraday variability over timescales in a range of 0.14 day (S5 0716+714) to 0.98 day (PKS 2155–304);

(2) For the 16 sources with enough observations, 12 sources show bluer spectrum when they are brighter, suggesting a BWB property in the optical band, three sources show the RWB phenomenon, and one source does not show any brightness-dependent tendency;
(3) Doppler factors are estimated for those sources. The optical polarization and the Doppler factor follow the Doppler factor-polarization relation, suggesting that the polarization depends on the Doppler factor;
(4) The optical variation amplitude is correlated with the variation of color index, which is consistent with the BWB phenomenon;
(5) The optical variation amplitude is correlated with the optical polarization, suggesting both parameters can be regarded as beaming effect indicators.

Acknowledgments

The work is partially supported by the National Natural Science Foundation of China (NSFC, grant Nos. U2031201, 12433004, 11733001, U2031112, 12133004, and 12103012), and Guangdong Major Project of Basic and Applied Basic Research (grant No. 2019B030302001). We also acknowledge the science research grants from the China Manned Space Project with NO. CMS-CSST-2021-A06, and the supports for Astrophysics Key Subjects of Guangdong Province and Guangzhou City. The work is also supported by the Key Laboratory for Astronomical Observation and Technology of Guangzhou. The authors thank the referee for providing helpful comments and detailed remarks.

ORCID iDs

Le-Jian Ou https://orcid.org/0009-0000-4469-3177

References

Abdo, A. A., Ackermann, M., Agudo, I., et al. 2010, ApJ, 716, 30
Abdollahi, S., Acero, F., Ackermann, M., et al. 2020, ApJS, 247, 33
Acero, F., Ackermann, M., Ajello, M., et al. 2015, ApJS, 218, 23
Ajello, M., Angioni, R., Axelsson, M., et al. 2020, ApJ, 892, 105
Aleksić, J., Antonelli, L. A., Antoranz, P., et al. 2011, ApJL, 730, L8
Bachev, R., Tripathi, T., Gupta, A. C., et al. 2023, MNRAS, 522, 3018
Ballet, J., Burnett, T. H., Digel, S. W., & Lott, B. 2020, arXiv:2005.11208
Burstein, D., & Heiles, C. 1982, AJ, 87, 1165
Cai, J. T., Kurtanidze, S. O., Liu, Y., et al. 2022, ApJS, 260, 47
Caproni, A., & Abraham, Z. 2004, MNRAS, 349, 1218
Carnerero, M., Raiteri, C., Villata, M., et al. 2017, MNRAS, 472, 3789
Chang, Y. L., Arsioli, B., Giommi, P., & Padovani, P. 2017, A&A, 598, A17
Chen, L. 2018, ApJS, 235, 39
Chen, Y., Gu, Q., Fan, J., et al. 2022, RAA, 22, 095006
Chen, Y., Gu, Q., Fan, J., et al. 2023, MNRAS, 519, 6199
Cheng, K. S., Fan, J. H., & Zhang, L. 1999, A&A, 352, 32
Costamante, L., & Ghisellini, G. 2002, A&A, 384, 56
Costamante, L., Ghisellini, G., Giommi, P., et al. 2001, A&A, 371, 512
Fan, J. 2003, ApJL, 585, L23
Fan, J., Xiao, H., Yang, W., et al. 2023, ApJS, 268, 23
Fan, J.-H. 2005, A&A, 436, 799
Fan, J.-H., Bastieri, D., Yang, J.-H., et al. 2014, RAA, 14, 1135
Fan, J. H., Cheng, K. S., Zhang, L., & Liu, C. H. 1997, A&A, 327, 947
Fan, J.-H., Hua, T.-X., Yuan, Y.-H., et al. 2006, PASJ, 58, 945
Fan, J. H., Kurtanidze, S. O., Liu, Y., et al. 2021, ApJS, 253, 10
Fan, J. H., & Lin, R. G. 2000, ApJ, 537, 101
Fan, J. H., Lin, R. G., Xie, G. Z., et al. 2002, A&A, 381, 1
Fan, J.-H., Romero, G. E., Wang, Y.-X., & Zhang, J.-S. 2005, ChJAA, 5, 457
Fan, J.-H., Yang, J.-H., Liu, Y., & Zhang, J.-Y. 2013, RAA, 13, 259
Fan, J. H., Yang, J. H., Liu, Y., et al. 2016, ApJS, 226, 20
Fan, J.-H., Yuan, Y.-H., Liu, Y., et al. 2008, PASJ, 60, 707
Fang, Y., Chen, Q., Zhang, Y., & Wu, J. 2022, ApJ, 933, 224
Feigelson, E., Bradt, H., McClintock, J., et al. 1986, ApJ, 302, 337
Foschini, L., Ghisellini, G., Tavecchio, F., Bonnoli, G., & Stamerra, A. 2011, A&A, 530, A77
Gaur, H., Gupta, A. C., Bachev, R., et al. 2019, MNRAS, 484, 5633
Ghisellini, G. 1998, arXiv:astro-ph/9812419
Ghisellini, G., Celotti, A., Fossati, G., Maraschi, L., & Comastri, A. 1998, MNRAS, 301, 451
Ghisellini, G., Tavecchio, F., Foschini, L., et al. 2012, MNRAS, 425, 1371
Ghisellini, G., Tavecchio, F., Maraschi, L., Celotti, A., & Sbarrato, T. 2014, Natur, 515, 376
Graham, M. J., Djorgovski, S. G., Stern, D., et al. 2015, Natur, 518, 74
Gu, M. F., Lee, C. U., Pak, S., Yim, H. S., & Fletcher, A. B. 2006, A&A, 450, 39
Gupta, A. C., Gaur, H., Wiita, P. J., et al. 2019, AJ, 157, 95
Gupta, A. C., Tripathi, A., Wiita, P. J., et al. 2018, A&A, 616, L6
Hartman, R. C., Bertsch, D. L., Bloom, S. D., et al. 1999, ApJS, 123, 79
Hovatta, T., Valtaoja, E., Tornikoski, M., & Lähteenmäki, A. 2009, A&A, 494, 527
Jorstad, S. G., Marscher, A. P., Raiteri, C. M., et al. 2022, Natur, 609, 265
Kalita, N., Yuan, Y., Gu, M., et al. 2023, ApJ, 943, 135
Lähteenmäki, A., & Valtaoja, E. 1999, ApJ, 521, 493
Li, T., Wu, J.-H., Meng, N.-K., Dai, Y., & Zhang, X.-Y. 2021, RAA, 21, 259
Liang, J., Zeng, X., Chen, G., et al. 2023, PASP, 135, 084103
Liao, N., Bai, J., Liu, H., et al. 2014, ApJ, 783, 83
Lin, C., & Fan, J.-H. 2016, RAA, 16, 103
Lind, K. R., & Blandford, R. D. 1985, ApJ, 295, 358
Liodakis, I., Hovatta, T., Huppenkothen, D., et al. 2018, ApJ, 866, 137
Lu, L., Zhou, W.-L., Luo, G.-Y., & Sun, B. 2023, RAA, 23, 015012
Massaro, F., Paggi, A., Errando, M., et al. 2013, ApJS, 207, 16
Mattox, J. R., Bertsch, D. L., Chiang, J., et al. 1993, ApJ, 410, 609
Mead, A., Ballard, K., Brand, P., et al. 1990, A&AS, 83, 204
Meng, N., Zhang, X., Wu, J., Ma, J., & Zhou, X. 2018, ApJS, 237, 30
Nieppola, E., Tornikoski, M., & Valtaoja, E. 2006, A&A, 445, 441
Otero-Santos, J., Acosta-Pulido, J. A., Becerra González, J., et al. 2020, MNRAS, 492, 5524
Otero-Santos, J., Peñil, P., Acosta-Pulido, J. A., et al. 2023, MNRAS, 518, 5788
Padovani, P., & Giommi, P. 1995, ApJ, 444, 567
Paliya, V. S., Domínguez, A., Ajello, M., Olmo-García, A., & Hartmann, D. 2021, ApJS, 253, 46
Pei, Z., Fan, J., Yang, J., & Bastieri, D. 2020, PASA, 37, e043
Pei, Z., Fan, J., Yang, J., Huang, D., & Li, Z. 2022, ApJ, 925, 97
Poon, H., Fan, J., & Fu, J. 2009, ApJS, 185, 511
Raiteri, C., Villata, M., Jorstad, S., et al. 2023, MNRAS, 522, 102
Romero, G. E., Chajet, L. S., Abraham, Z., & Fan, J. H. 2000, A&A, 360, 64
Savolainen, T., Homan, D. C., Hovatta, T., et al. 2010, A&A, 512, A24
Seaton, M. J. 1979, MNRAS, 187, 73
Shaw, M. S., Romani, R. W., Cotter, G., et al. 2012, ApJ, 748, 49
Smith, P. S., Montiel, E., Rightley, S., et al. 2009, arXiv:0912.3621
Urry, C. M., & Padovani, P. 1995, PASP, 107, 803
Villata, M., Raiteri, C. M., Balonek, T., et al. 2006, A&A, 453, 817
von Montigny, C., Bertsch, D. L., Chiang, J., et al. 1995, ApJ, 440, 525
Wakely, S. P., & Horan, D. 2008, ICRC (Mérida), 3, 1341
Wang, G. G., Cai, J. T., & Fan, J. H. 2022, ApJ, 929, 130
Wang, H., Yin, C., & Xiang, F. 2017, Ap&SS, 362, 99
Wang, H.-T., & Shi, Y. 2020, RAA, 20, 021
Wills, B. J., Wills, D., Breger, M., Antonucci, R. R. J., & Barvainis, R. 1992, ApJ, 398, 454
Wu, J., Zhou, X., Ma, J., & Jiang, Z. 2011, MNRAS, 418, 1640
Xiang, M., Shi, J., Liu, X., et al. 2018, ApJS, 237, 33

Xiao, H., Fan, J., Ouyang, Z., et al. 2022, ApJ, 936, 146
Xiao, H., Fan, J., Yang, J., et al. 2019, SCPMA, 62, 129811
Xie, G. Z., Li, K. H., Liu, F. K., et al. 1992, ApJS, 80, 683
Xie, G. Z., Lu, J. F., Wu, J. X., Lu, R. W., & Hao, P. J. 1989, A&A, 220, 89
Xiong, D., Bai, J., Zhang, H., et al. 2017, ApJS, 229, 21
Yang, J., Fan, J., Liu, Y., et al. 2023, SCPMA, 66, 249511
Yang, J. H., Fan, J. H., Liu, Y., et al. 2017, Ap&SS, 362, 219
Yang, J. H., Fan, J. H., Liu, Y., et al. 2022, ApJS, 262, 18
Yang, W. X., Wang, H. G., Liu, Y., et al. 2022a, ApJ, 925, 120
Yang, W.-X., Xiao, H.-B., Wang, H.-G., et al. 2022b, RAA, 22, 085002
Yu, J., Ding, N., Fan, J., Tang, Y., & Cao, J. 2024, ApJ, 967, 96
Yuan, Y., Du, G., Fan, J., et al. 2023, ApJS, 269, 60
Yuan, Y. H., Wang, G. G., Xiao, H. B., et al. 2022, ApJS, 262, 43
Zhai, M., Zheng, W. K., & Wei, J. Y. 2011, A&A, 531, A90
Zhang, B.-K., Tang, W.-F., Wang, C.-X., et al. 2023, MNRAS, 519, 5263
Zhang, L., Chen, S., Xiao, H., Cai, J., & Fan, J. 2020, ApJ, 897, 10
Zhang, L., Liu, Y., & Fan, J. 2022, ApJ, 935, 4
Zhang, L. X., & Fan, J. H. 2018, Ap&SS, 363, 142
Zhang, P.-F., Zhang, P., Liao, N.-H., et al. 2018, ApJ, 853, 193
Zhang, X., Wu, J., & Meng, N. 2018, MNRAS, 478, 3513
Zheng, Y. G., Zhang, X., Bi, X. W., Hao, J. M., & Zhang, H. J. 2008, MNRAS, 385, 823
Zhou, R. X., Zheng, Y. G., Zhu, K. R., & Kang, S. J. 2021, ApJ, 915, 59
Zhu, J. T., Lin, C., Xiao, H. B., et al. 2023, ApJ, 950, 123